

Isotope implications of groundwater recharge, residence time and hydrogeochemical evolution of the Longdong Loess Basin, Northwest China

LING Xinying^{1,2*}, MA Jinzhu¹, CHEN Peiyuan¹, LIU Changjie², Juske HORITA^{2*}

¹ Key Laboratory of Western China's Environmental System (Ministry of Education), Lanzhou University, Lanzhou 730000, China;

² Department of Geosciences, Texas Tech University, Lubbock TX79409, USA

Abstract: Groundwater plays a dominant role in the eco-environmental protection of arid and semi-arid regions. Understanding the sources and mechanisms of groundwater recharge, the interactions between groundwater and surface water and the hydrogeochemical evolution and transport processes of groundwater in the Longdong Loess Basin, Northwest China, is of importance for water resources management in this ecologically sensitive area. In this study, 71 groundwater samples (mainly distributed at the Dongzhi Tableland and along the Malian River) and 8 surface water samples from the Malian River were collected, and analysis of the aquifer system and hydrological conditions, together with hydrogeochemical and isotopic techniques were used to investigate groundwater sources, residence time and their associated recharge processes. Results show that the middle and lower reaches of the Malian River receive water mainly from groundwater discharge on both sides of valley, while the source of the Malian River mainly comes from local precipitation. Groundwater of the Dongzhi Tableland is of a $\text{HCO}_3\text{--Ca--Na}$ type with low salinity. The reverse hydrogeochemical simulation suggests that the dissolution of carbonate minerals and cation exchange between Ca^{2+} , Mg^{2+} and Na^+ are the main water-rock interactions in the groundwater system of the Dongzhi Tableland. The $\delta^{18}\text{O}$ (from -11.70‰ to -8.52‰) and $\delta^2\text{H}$ (from -86.15‰ to -65.75‰) values of groundwater are lower than the annual weighted average value of precipitation but closer to summer-autumn precipitation and soil water in the unsaturated zone, suggesting that possible recharge comes from the summer-autumn monsoonal heavy precipitation in the recent past (≤ 220 a). The corrected ^{14}C ages of groundwater range from 3,000 to 25,000 a old, indicating that groundwater was mainly from precipitation during the humid and cold Late Pleistocene and Holocene periods. Groundwater flows deeper from the groundwater table and from the center to the east, south and west of the Dongzhi Tableland with estimated migration rate of 1.29–1.43 m/a. The oldest groundwater in the Quaternary Loess Aquifer in the Dongzhi Tableland is approximately 32,000 a old with poor renewability. Based on the $\delta^{18}\text{O}$ temperature indicator of groundwater, we speculate that temperature of the Last Glacial Maximum in the Longdong Loess Basin was 2.4°C – 6.0°C colder than the present. The results could provide us the valuable information on groundwater recharge and evolution under thick loess layer, which would be significative for the scientific water resources management in semi-arid regions.

Keywords: groundwater recharge; hydrogeochemical evolution; isotope technology; ^{14}C dating; paleoclimate; residence time; Chinese Loess Plateau

*Corresponding author: LING Xinying (E-mail: lingxinying2009@126.com); Juske HORITA (E-mail: juske.horita@ttu.edu)

Received 2021-04-07; revised 2021-07-17; accepted 2021-08-06

© Xinjiang Institute of Ecology and Geography, Chinese Academy of Sciences, Science Press and Springer-Verlag GmbH Germany, part of Springer Nature 2022

Citation: LING Xinying, MA Jinzhu, CHEN Peiyuan, LIU Changjie, Juske HORITA. 2022. Isotope implications of groundwater recharge, residence time and hydrogeochemical evolution of the Longdong Loess Basin, Northwest China. *Journal of Arid Land*, 14(1): 34–55. <https://doi.org/10.1007/s40333-022-0051-7>

1 Introduction

Groundwater, approximately accounting for 96% of freshwater on the Earth except for glaciers (Shiklomanov and Rodda, 2003), is an essential global strategic resource and plays an important role in economic development as well as ecological balance. As the crisis of global water resources intensifies, especially in arid and semi-arid regions, where surface water resources are limited, the imbalance between water supply and demand, water pollution, the deterioration of ecological environments and other problems are increasingly prominent (Edmunds et al., 2006; Jia et al., 2021). In those regions, groundwater has been increasingly exploited and utilized to meet urgent need for the sustainability of society (Ragab and Prudhomme, 2002; Xia and Zhang, 2008; Pang et al., 2020; Cigna and Tapete, 2021). In addition to human activities, groundwater systems also respond to and record external, long-term natural factors such as regional to global climate changes (Walling and Fang, 2003; Ye et al., 2003; Christensen et al., 2004; Liu and Xia, 2004; Choi et al., 2005; Conway, 2005; Magilligan and Nislow, 2008; Amanambu et al., 2020; Patil et al., 2020). Understanding the property of groundwater resources, and their recharge and transport processes could contribute to science-based management and sustainable development of water resources on regional to global scales (Kinzelbach et al., 2003; Wheeler et al., 2010).

The Longdong Loess Basin, located on the Chinese Loess Plateau, is an important national energy industry base. Petroleum industry brings not only economic development, but also serious environmental problems. The leakage from oil wells and transport lines, and the discharge of wastewater and petroleum products heavily affect the quality of surface water and shallow groundwater. Since the 1990s, the total amount of wastewater discharged by petroleum industry into the Malian River reached $1.14 \times 10^7 \text{ m}^3$, which accounts for 63% of the total wastewater discharge of Qingyang, Gansu Province, China. Hexavalent chromium, volatile phenol and sulfate of Malian River were detected in 2013, and the values were all above the regulatory limits (Pan et al., 2014). As surface water is heavily polluted and not usable, groundwater has become the main water resource for economic development and human life in the Longdong Loess Basin. Recently, with the increasing exploitation of groundwater, a series of problems have emerged, including the decline of groundwater levels and groundwater pollution (Li, 2013). Li (2014) found that the amount of groundwater exploitation in the Dongzhi Tableland in 2011 was three times that in 1979, and groundwater levels at some areas have declined 12 m in the past 24 a. If this trend continues, further deterioration of ecosystems in the Dongzhi Tableland and even in the Longdong Loess Basin will be unavoidable (Li et al., 2014). Furthermore, the time required for annual precipitation to reach the groundwater table ranges from decades to hundreds of years, and the recharge (3.0×10^7 – $3.2 \times 10^7 \text{ m}^3/\text{a}$) through the thick unsaturated loess layer contributes so little to the groundwater system in the Dongzhi Tableland (Huang et al., 2020). Therefore, comprehensive studies on groundwater resources, hydrogeochemical evolution and groundwater flow mechanisms based on multi-tracers and multi-techniques are urgently needed to provide scientific guidance for the exploitation and management of groundwater resources and the protection of environment (Ma et al., 2013).

In the recent decades, studies of groundwater evolution and recharge processes have caught attentions of hydrologists and scientists (Edmunds et al., 2003, 2006; Ma and Edmunds, 2006). For instance, several geochemical tracers have been utilized to analyze groundwater recharge and residence time in North Africa, which can help to evaluate groundwater resources and understand the environmental and climatic change processes (Edmunds et al., 2003). Groundwater evolution and its controlling factors were analyzed in Arabia, and the similarity of hydrogen and oxygen isotopes indicated the same source of groundwater (Murad et al., 2011). Noble gases were used to estimate the age of deep paleo-groundwater and brine in the Baltic Artesian Basin (Gerber et al., 2017). Cochand et al. (2020) determined the rapid groundwater recharge dynamics in permafrost

watershed of Nunavik based on the combination of hydrogeochemical and isotopic tracers. Jesiya et al. (2021) used stable isotope ratios to solve the problems related to groundwater systems in coastal cities in southern India. Obeidat et al. (2021) identified the source of nitrate in the upper aquifer system of the Wadi Shueib Catchment in Jordan using stable isotope analysis method. In Northwest China, based on a wide range of geochemical tracers, it was found that local groundwater in the Minqin Basin had received a supply of water under a cold and wet period from the Late Pleistocene to Holocene (Edmunds et al., 2006). Hydrological and hydrochemical processes were analyzed in groundwater-fed oasis under arid climate (Wang et al., 2020). Groundwater flow paths, recharge processes, as well as groundwater ages were studied by using isotopes in multiple researches (Wang et al., 2020; Zhang et al., 2020). In the Longdong Loess Basin, Jia (2010) compared the components of groundwater before and after the 2000s and analyzed the influence of petroleum pollutants on groundwater and its geochemical evolution characteristics. Li (2013) studied the groundwater dynamics of the Dongzhi Tableland and found that the declining groundwater levels were resulted from decreasing recharge rate and the increasing exploitation rate of groundwater. Although studies on the quality and quantity of groundwater characteristics in the Longdong Loess Basin were carried out, the complex groundwater system, recharge mechanisms and renewability are still poorly understood.

The main objective of this study is to reveal the characteristics of hydrogeochemical evolution, groundwater recharge sources, residence times and migration rates, and paleoclimate characteristics of groundwater in the Longdong Loess Basin by a combination of geochemical tracer techniques, such as chemical compositions of dissolved ions, hydrogen and oxygen stable isotopes of water, and radiocarbon dating of dissolved CO₂ species. These results could not only contribute to the understanding of the groundwater system in the Longdong Loess Basin, but also provide science-based support and guidance for the regional management of groundwater resources and water sustainability.

2 Study area

2.1 General setting

The Longdong Loess Basin (34°54'–37°10'N, 106°21'–108°45'E) is located in the east part of Gansu Province, China; it is bounded by the Ziwuling Mountain to the east, the Liupan Mountains to the west, the Yangjuan Mountain to the north and the Guanzhong Plain to the south (Fig. 1). The total area is 3.34×10^4 km² with the altitude between 1200–1800 m. Hills, gullies and tablelands are the main landforms of the Longdong Loess Basin. The Dongzhi Tableland located between the Puhe River and Malian River within the Longdong Loess Basin is the largest (1042 km²) and the best-preserved tableland in China (Li et al., 2014). It is also a main crop production area, called the "Longdong Granary".

The study area has a temperate continental monsoon climate with obvious seasonal variations. The annual average temperature is about 10.0 °C, with the highest temperature of 38.4 °C and the lowest of –22.0 °C. The total solar radiation is about 525 to 610 kJ/m². Northwest wind prevails in winter and southeast wind in summer. The precipitation increases from northwest to southeast with the average annual precipitation of around 505 mm. It also varies among seasons: nearly 60% annual precipitation occurs as rainstorms in July, August and September. The source of water vapor for the study area is a mixture of Bay of Bengal, southeast monsoon, westerly zone vapor and local re-evaporated water vapor in summer months, while in winter months, water vapor from westerly zone dominates (Liu et al., 2008; Liu et al., 2019). The potential evaporation ranges from 1380 to 1750 mm, increasing from south to north.

2.2 Hydrogeology

The Longdong Loess Basin, as part of the front delta developed in the southwest margin of an alluvial fan of the Ordos Basin, was formed in the Mesozoic (Liang, 2011). The stone layers, nearly horizontal Tertiary Mudstone and Cretaceous Sandstone, are deposited

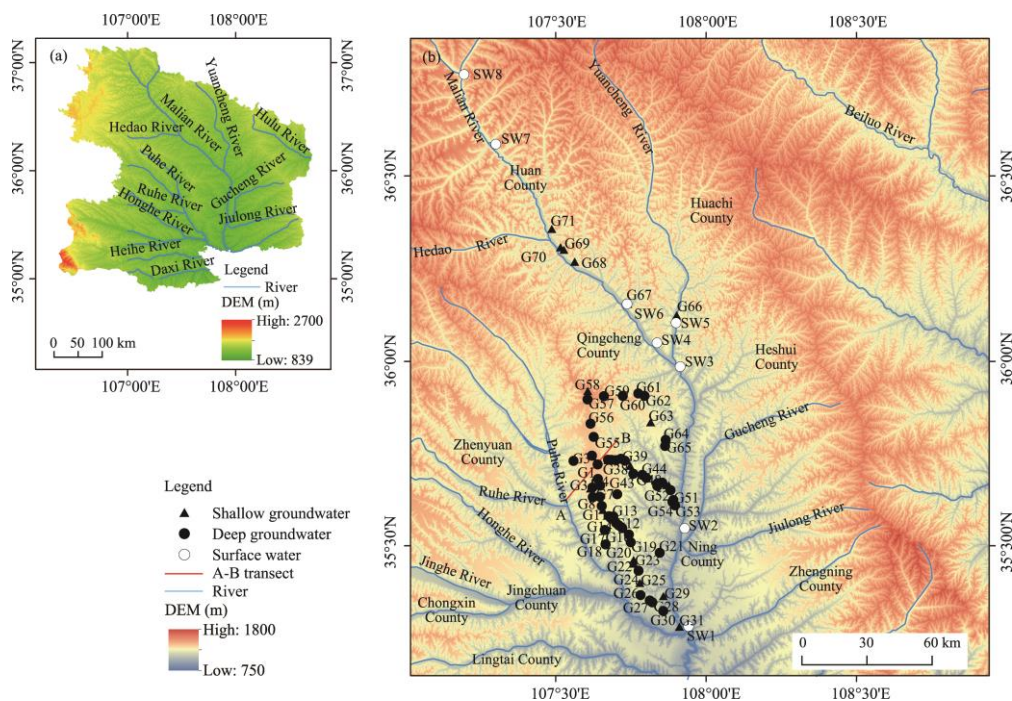


Fig. 1 Overview of the Longdong Loess Basin (a) and sample location (b). G1–G71, groundwater samples; SW1–SW8, surface water samples. A represents Pengyang village, B represents Gaolou village, and the line between A and B represents the geological profile of A-B transect showed in Figure 2. DEM, digital elevation model.

below the Quaternary Loess Strata, which are thick (170–250 m) and widespread in the whole Longdong Loess Basin (Fig. 2). The Quaternary Loess Strata includes the Lower Pleistocene Series, the Middle Pleistocene Series, the Upper Pleistocene Series and the Holocene Series Strata. The Lower Pleistocene Series Strata is characterized as the orange sandy clay with paleosol, about 40–60 m thick. It is regarded as an impermeable layer because of its compact and rigid structure. The Middle Pleistocene Series Stone Loess with 120–150 m thickness is characterized as the grayish yellow and light red silty soil and outcropped only at the edges of the Dongzhi Tableland. It is homogeneous and unconsolidated with macropores and vertical joint structures, and is the main unconfined aquifer of the Dongzhi Tableland. The Upper Pleistocene Series Strata includes the Malan Loess with the thickness of around 10 m, which deposits as homogeneous floury soil, containing macropores and vertical joint structures. There is an alluvium strata at the triple terraces of riverside, mainly consisting of loess silt with silty-fine sand and sandy gravel stratum. The Holocene Series Strata with 1–5 m thick silts mainly consists of alluvial deposits; it is distributed on the first and second terraces of riverside. The Quaternary Loess Strata consists largely of silt loam with the mineralogy of mainly quartz, feldspar, mica, carbonate (calcite and dolomite) and clay minerals (kaolinite and smectite) (Liu, 1985; Zheng et al., 1994).

The Dongzhi Tableland is an independent hydrogeological unit, bordered by the Malian River to the east and the Puhe River to the west. The Quaternary Loess Strata of the Dongzhi Tableland is relatively horizontal and incised by many deep valleys; surface water flows on the groove of valleys. The precipitation is the only supply for the unconfined groundwater in the Dongzhi Tableland (Wang and Liu, 2005). The infiltration pathway in the unsaturated zone is piston flow with a soil water infiltration velocity of 0.12–0.14 m/a and a recharge rate of 37–41 mm/a in the study area (Huang et al., 2020). An unconfined groundwater is stored in pores and fissures of the Middle Pleistocene Series Stone Loess. The Wucheng Loess layer contained in the Lower Pleistocene Series Strata and beneath the unconfined aquifer is impermeable, generally acting as an aquitard with limited connections through macrovoid, fissure and vertical joint structure. The

depths of the groundwater table increase from approximately 30 m at the center to 100 m at the margin of the Dongzhi Tableland. The thickness of the unconfined aquifer decreases from 40–80 m at the center to less than 40 m at the margin. With the slow recharge rate and thick unsaturated zone, the infiltration time for precipitation to reach the groundwater table is hundreds of years (Huang et al., 2020).

Hydraulic conductivity of the unconfined aquifer ranges between 0.14 and 0.46 m/d (Jia, 2010) and specific yield is from 0.02 to 0.10 (Qu, 1991; Li, 1999; Li et al., 2014). Groundwater gradients increase from the center region (8.5×10^{-3}) to the margin (3.3×10^{-2}), and pumping yield of a single well decreases from the center to margin (Li et al., 2014). The unconfined groundwater of the Dongzhi Tableland flows from the center to the margin as divergent planar flow and discharges as springs and rivers to the valleys (Pan et al., 2012), because the groundwater level along the Malian River is higher than the river level (Su et al., 2009; Wang et al., 2018). The poor quality of the Malian River, especially in the north with very high total dissolved solids (TDS), is improved along the flow path, as it receives the supply from tributaries and groundwater with better quality.

The confined groundwater is contained in the Cretaceous Luohe Group, the Huanhe Group and the Luohandong Group, consisting of sandstone, argillaceous sandstone and sandy mudstone. The depth of the confined groundwater is more than 300 m in the Dongzhi Tableland and 10–30 m along the Malian River. For the strata with relatively permeable sandstone, its hydraulic connection between surface water and groundwater is relatively strong, and its groundwater discharges to surface water. Otherwise, the confined groundwater can hardly discharge.

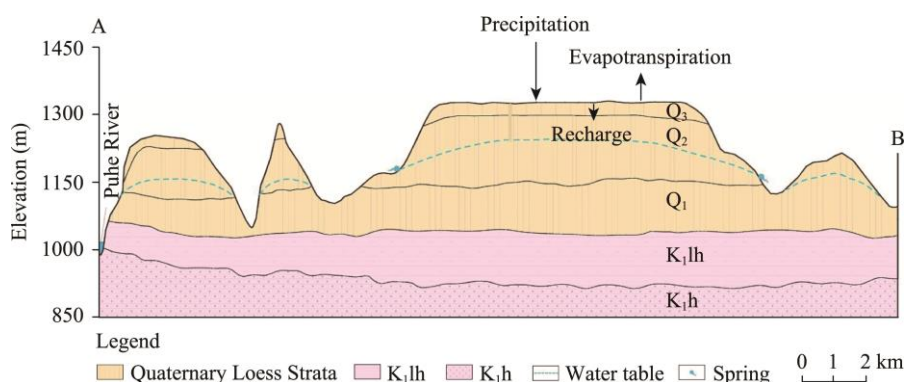


Fig. 2 Geological cross-section along A–B transect of the Dongzhi Tableland (modified from Huang et al. (2020)). K₁h, Cretaceous Sandstone; K₁lh, Tertiary Mudstone; Q₁, Lower Pleistocene Series Wucheng Loess; Q₂, Middle Pleistocene Series Stone Loess; Q₃, Upper Pleistocene Series Malan Loess.

3 Materials and methods

Based on the previous studies (Ma et al., 2004, 2005, 2006, 2013) and the hydrogeological background of the study area, we collected 79 water samples from the Longdong Loess Basin from July to August in 2018 and 2019, including 71 groundwater samples (G1–G71; mainly distributed in the Dongzhi Tableland and along the Malian River) and 8 surface water samples (SW1–SW8) from the Malian River (Fig. 1). The depth of samples, geographical location, and the conditions of surroundings were recorded (Fig. 1; Table S1). Based on the hydrogeological characteristics, hydraulic property, aquifer medium and groundwater depth, we defined the groundwater with depth less than 100 m as shallow groundwater and groundwater deeper than 100 m as deep groundwater. In the field, water had been pumped from the wells for more than 2 h and then groundwater samples were collected. All water samples were collected into polyethylene sample bottles; these bottles were washed three times by deionized water in advance. A sensION156 portable multi-parameter meter (Hach, Loveland, Colorado, USA) was used to measure the temperature, pH, TDS, specific electrical conductivity (SEC) of groundwater and

surface water samples in the field.

Alkalinity was measured by a digital titrator (Model 16900, Hach, Loveland, Colorado, USA) with a precision of $\pm 1\%$ standard deviation, using a bromocresol green-methyl red indicator; it was then converted into the concentration of HCO_3^- . Water samples were filtered through a $0.45\text{-}\mu\text{m}$ membrane filter and divided into 3 subsamples, with 2 stored in acid-washed, well-rinsed and dried 20 mL polyethylene bottles for chemical analysis, and 1 stored in 2 mL glass vial for isotope measurement. The subsample used to determine cations was acidified with 1% HNO_3 to a pH value of around 1.5 to stabilize the metals and prevent deposition. The subsample used to determine anions and stable isotopes was not acidified. Unfiltered 1.5 L water samples were collected for the radiocarbon analysis. Water samples were stored in refrigerator with temperature of $4\text{ }^\circ\text{C}$ until measurement.

Chemical and isotopic measurements were carried out at Key Laboratory of Western China's Environmental System, Lanzhou University, China soon after the fieldwork. The concentrations of major ions (Ca^{2+} , Na^+ , K^+ , Mg^{2+} , SO_4^{2-} , Cl^- , NO_3^- and F^-) were analyzed by ICS-2500 ion chromatography (Dionex, Sunnyvale, California, USA) with an analytical precision of $\pm 3\%$ and a detection limit of 0.01 mg/L . Appropriately diluted standards from both laboratory and international references were used for calibration. Charge balance agreed within $\pm 5\%$ for most water samples. We used PHREEQC (USGS, USA) to calculate the saturation index (SI), which is based on the ionic association and Debye-Huckel theory.

The $\delta^2\text{H}$ and $\delta^{18}\text{O}$ of groundwater and surface water samples were measured by Picarro L2130-i (Picarro Inc., Santa Clara, California, USA) at Key Laboratory of Western China's Environmental System with the accuracy errors lower than $\pm 0.1\text{‰}$ and $\pm 0.025\text{‰}$, respectively. Each sample was measured for six times with the first three measurements discarded to remove memory effect, and the result was an average of the last three measurements. Isotope results were presented relative to the Vienna Standard Mean Ocean Water (VSMOW). Sixty sets of the $\delta^{18}\text{O}$ and $\delta^2\text{H}$ values of monthly precipitation in the period of 1985–1993 were obtained from the Xi'an Station of Global Network of Isotopes in Precipitation, International Atomic Energy Agency, which is located approximately 200 km southeast of the Dongzhi Tableland. Due to the lack of long-term precipitation isotope data in the study site, we assumed those data gathered in Xi'an can represent the condition of the Dongzhi Tableland.

Radiocarbon samples (G2, G22, G30, G35, G43, G47, G59 and G65) were analyzed at Australian National University, Australia. Dissolved inorganic carbon (DIC) was reacted with 85% phosphoric acid to convert first to CO_2 and then to graphite. The ^{14}C was measured by an accelerator mass spectrometer (AMS) (Thermo Fisher Scientific Inc., Waltham, Massachusetts, USA) with an error less than 0.22 pmC (percent modern carbon). The $\delta^{13}\text{C}$ of DIC was measured by an isotope ratio mass spectrometer (IRMS) (Thermo Fisher Scientific Inc., Waltham, Massachusetts, USA) with an overall analytical error of $\pm 0.15\text{‰}$. In addition, we also included the radiocarbon data of 11 groundwater samples (XF3, XF5, XF6, XF9, XF11, XF14, XF16, XF20, XF22, XF24 and XF25) in the Dongzhi Tableland from Huang et al. (2020).

4 Results

4.1 Hydrogeochemical characteristics of surface water and groundwater

Setting sample G1 as the center location, groundwater samples in the study area are divided into four groups: the south line (G1–G31), east line (G32–G54), north line (G55–G65) and Malian River line (i.e., groundwater samples collected along the Malian River; G66–G71) (Fig. 1). TDS of the Dongzhi Tableland groundwater is low and relatively constant around $200\text{--}270\text{ mg/L}$. There is no obvious chemical grouping in the Dongzhi Tableland groundwater. However, compared with groundwater from the Dongzhi Tableland (G1–G65), the groundwater collected along the Malian River (G66–G71) and the river water (SW1–SW8) are highly mineralized, and their TDS contents decline from approximately 3500 to 450 mg/L (groundwater) and from 7400 to 800 mg/L (surface water) along northwest to southeast transect.

The cations of groundwater in the Dongzhi Tableland (the south, east and north lines) are mainly Ca^{2+} , followed by Na^+ , K^+ and Mg^{2+} , while the dominant anion is HCO_3^- (Fig. 3; Table S1). The cation and anion concentrations of groundwater in the Dongzhi Tableland vary among the south, east and north lines: Na^+ from 8.69 to 75.53 mg/L, K^+ from 0.30 to 2.21 mg/L, HCO_3^- from 127.00 to 308.00 mg/L and SO_4^{2-} from 0.98 to 15.99 mg/L. One of the most striking features is that the concentrations of Mg^{2+} and Ca^{2+} of groundwater in the Dongzhi Tableland vary along the two parallel linear trends, while the total concentration ($\text{Mg}^{2+} + \text{Ca}^{2+}$) falls along one linear trend (Fig. 3).

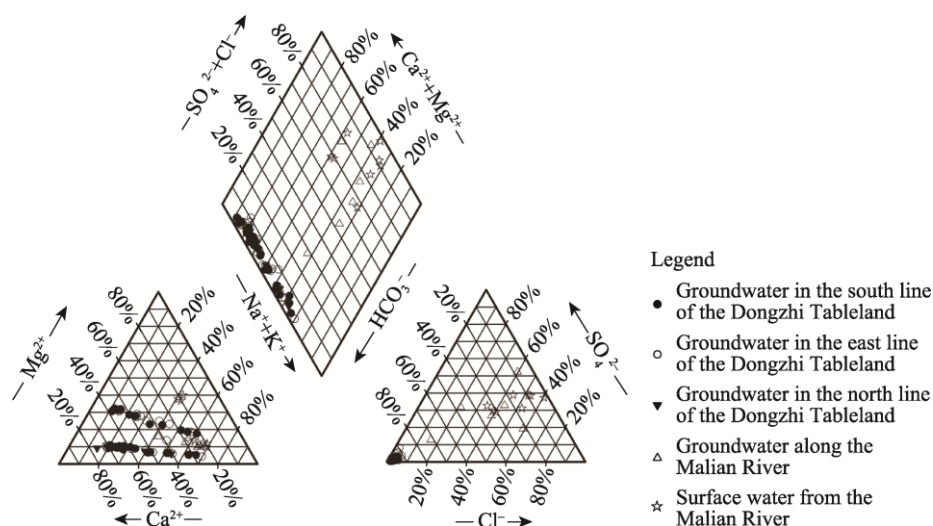


Fig. 3 Variations of ion concentrations in groundwater and surface water in the Longdong Loess Basin

The main cations of groundwater along the Malian River line and surface water of the Malian River are Na^+ and K^+ , and the anions are mainly Cl^- and SO_4^{2-} . The hydrochemical type of these groundwater changes from north to south: from $\text{SO}_4\text{--HCO}_3\text{--Na--Ca}$ in Huan County to $\text{Cl--HCO}_3\text{--Na--Ca}$ in Qingcheng County to $\text{HCO}_3\text{--Ca--Na}$ in the Dongzhi Tableland (mostly in Xifeng District) (Figs. 1 and 3). Surface water and groundwater along the Malian River show linear trends of growth between Cl^- and other ions (i.e., Na^+ , Ca^{2+} and SO_4^{2-}), with a notable exception of G71 groundwater (Fig. 4). Surface water samples (SW1, SW2 and SW3) in the downstream show elevated Mg^{2+} (Fig. 4).

Almost all groundwater samples are near or slightly above saturation with calcite, except for G2, G10 and G31. The SI data of dolomite are similar to those of calcite with larger fluctuation, which is probably influenced by the concentration of Mg^{2+} . Gypsum is far from saturation in groundwater of the Dongzhi Tableland because of low concentration of SO_4^{2-} . Compared with groundwater samples of the Dongzhi Tableland, those samples along the Malian River are different: the SI value of gypsum is larger than that of the Dongzhi Tableland, but it is still under saturated. It is likely that the concentrations of chemical ions of groundwater along the Malian River are higher than those of the Dongzhi Tableland.

4.2 Stable isotope compositions of surface water and groundwater

The distribution and characteristics of the $\delta^2\text{H}$ and $\delta^{18}\text{O}$ values of precipitation are sensitive to climate and local environment (Sklash, 1990). Precipitation during 2018–2019 in the Dongzhi Tableland yields the weighted average value of $\delta^{18}\text{O} = -8.50\text{‰}$ (Huang et al., 2020). Precipitation in the headwater region of the Malian River in 2000–2001 exhibits the weighted average values of $\delta^{18}\text{O} = -7.90\text{‰}$ and $\delta^2\text{H} = -54.42\text{‰}$ (Su et al., 2009). Sixty sets of the $\delta^{18}\text{O}$ and $\delta^2\text{H}$ values of monthly precipitation in the period of 1985–1993 are obtained from the Xi'an Station of Global Network of Isotopes in Precipitation, International Atomic Energy Agency, which is located approximately 200 km southeast of the Dongzhi Tableland. The local meteoric water line

(LMWL) of the Dongzhi Tableland ($\delta^2\text{H}=7.49\delta^{18}\text{O}+6.13$) and the weighted average values of modern precipitation ($\delta^2\text{H}= -49.13\text{‰}$ and $\delta^{18}\text{O}= -7.49\text{‰}$) are obtained from the Xi'an precipitation data (1985–1993; Fig. 5). There is small difference between the global meteoric water line (GMWL) and LMWL of Xi'an (Fig. 5).

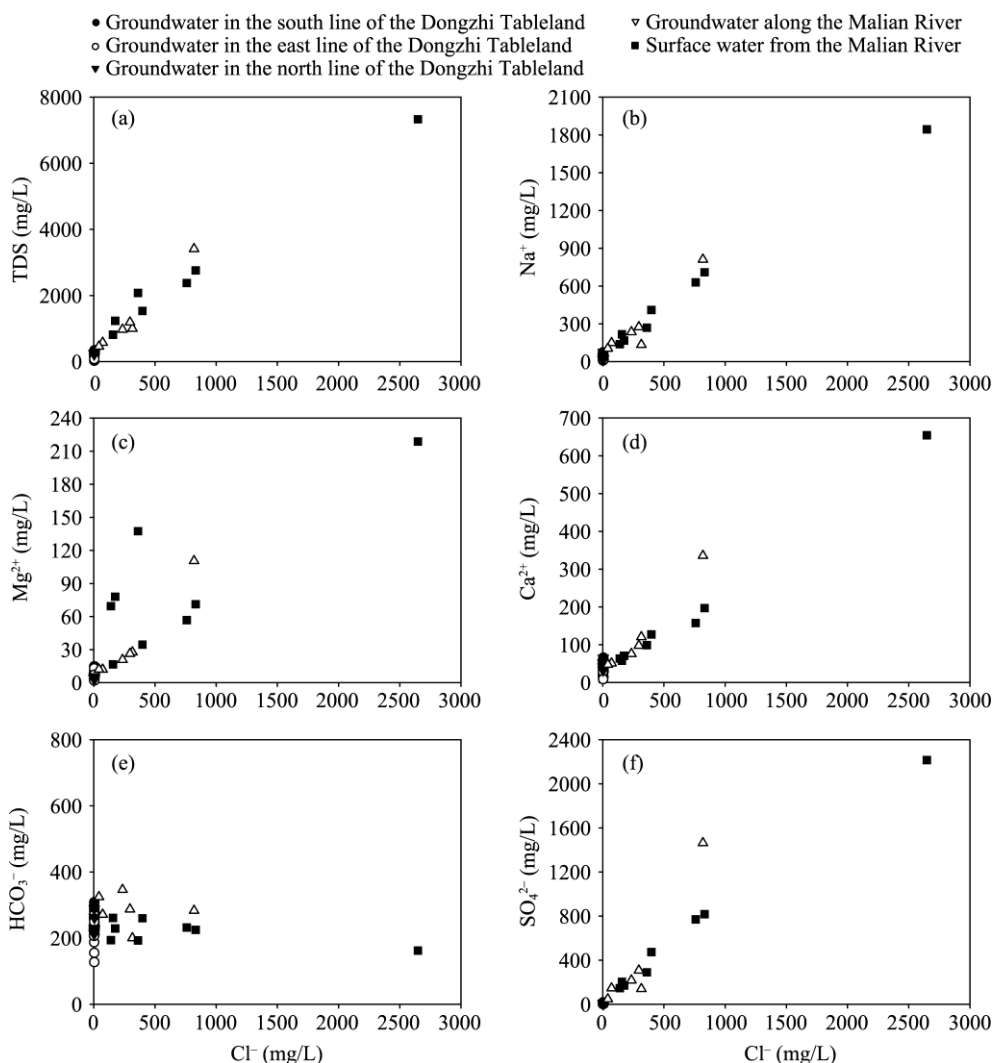


Fig. 4 Relationships of Cl^- with TDS (a) and major ions (b, c, d, e and f) of groundwater and surface water collected from the Longdong Loess Basin. TDS, total dissolved solids.

In the Dongzhi Tableland, the $\delta^{18}\text{O}$ of surface water varies from -9.44‰ to -7.01‰ , and the $\delta^2\text{H}$ ranges from -72.03‰ to -59.13‰ . The isotope compositions of surface water are slightly more enriched than those of groundwater with some deviations from the LMWL (Fig. 5). The $\delta^{18}\text{O}$ and $\delta^2\text{H}$ of surface water in the upstream of the Malian River (SW6–SW8) are more enriched, while surface water in the middle and lower reaches of the Malian River (SW1–SW5) have lower $\delta^{18}\text{O}$ and $\delta^2\text{H}$ values, which are close to those of groundwater. The isotope compositions of groundwater along the Malian River are lower with wider variations than those of groundwater in the Dongzhi Tableland (Fig. 6). From northwest to southeast along the Malian River, the $\delta^{18}\text{O}$ of groundwater generally becomes more depleted (Fig. 6).

The $\delta^{18}\text{O}$ of groundwater in the Dongzhi Tableland ranges from -11.70‰ to -8.52‰ and the $\delta^2\text{H}$ varies from -86.15‰ to -65.75‰ (Table S1). The variation trajectories of the $\delta^{18}\text{O}$ and $\delta^2\text{H}$ values are distributed along the LMWL (Fig. 5), which indicates that groundwater in the study

area originates from the meteoric precipitation. However, compared with the weighted average values of isotopes in modern precipitation in Xi'an ($\delta^2\text{H} = -49.13\text{‰}$ and $\delta^{18}\text{O} = -7.49\text{‰}$), isotopes in groundwater of the Dongzhi Tableland are depleted. The $\delta^{18}\text{O}$ of shallow groundwater is between -11.70‰ and -9.05‰ , with the weighted average value of -10.10‰ , and the $\delta^2\text{H}$ of shallow groundwater is between -86.15‰ and -68.95‰ , with the weighted average value of -73.05‰ . The $\delta^{18}\text{O}$ of deep groundwater is between -10.61‰ and -8.53‰ , with the weighted average value of -9.89‰ , and the $\delta^2\text{H}$ of deep groundwater is between -76.64‰ and -65.76‰ , with the weighted average value of -71.57‰ . The range of the isotope compositions of shallow groundwater is larger than that of deep groundwater. Datasets of the $\delta^{18}\text{O}$ and $\delta^2\text{H}$ values of groundwater from Huang et al. (2020) show similar variations with our results. There is little difference in the isotope compositions among groundwater of the south line, east line and north line in the Dongzhi Tableland. However, the range of the $\delta^2\text{H}$ in the east line is slightly larger than those in the south line and north line (Fig. 6).

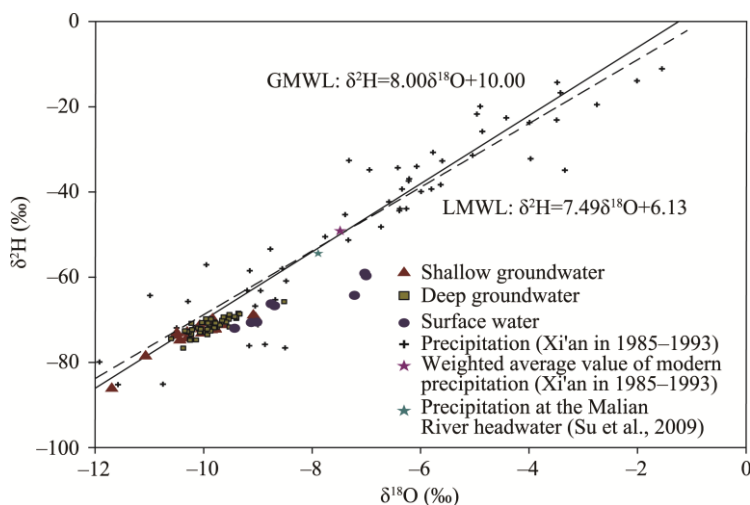


Fig. 5 $\delta^2\text{H}$ and $\delta^{18}\text{O}$ values of groundwater in the Dongzhi Tableland, surface water in the Malian River and precipitation in Xi'an and at the Malian River headwater. GMWL, global meteoric water line; LMWL, local meteoric water line.

4.3 ^{14}C -based age of groundwater

The measurement of groundwater age is important to understand its source and the process of recharge and drainage, as well as the transport characteristics. Many radioactive isotopes have been applied to the research of groundwater dating (Cook and Herczeg, 2000), ranging from a few decades (^3H , ^{85}Kr and $^3\text{He}/^3\text{H}$) to millions of years (^{129}I and ^{81}Kr). The ^{14}C (half-life of 5.73×10^3 a) of dissolved CO_2 (mainly in HCO_3^- and CO_3^{2-} forms) in groundwater can be used to date groundwater in the range of 1000 to 10,000 a (Godwin, 1962). Many researches on radiocarbon dating have been carried out in Northwest China (Edmunds et al., 2006; Zhu et al., 2008; Ma et al., 2010).

In this study, Vogel Model (Vogel, 1967), Tamers Model (Tamers, 1966), Chemical Mass Balance (CMB) Model (Fontes and Garnier, 1979), improved Pearson Model (Pearson and Hanshaw, 1970) and Fontes-Garnier (F-G) Model (Fontes and Garnier, 1979) were used to correct the initial radiocarbon concentrations of eight groundwater samples (G2, G22, G30, G35, G43, G47, G59 and G65) collected from the Dongzhi Tableland and 11 groundwater samples (XF3, XF5, XF6, XF9, XF11, XF14, XF16, XF20, XF22, XF24 and XF25) from Huang et al. (2020). All groundwater samples from Huang's analysis were detected tritium-free. We set the $\delta^{13}\text{C}$ values of soil CO_2 and solid carbonate as -23.00‰ and 0.00‰ , respectively. The ^{14}C values of soil CO_2 and solid carbonate were assumed as 100.00 and 0.00 pmC, respectively (Clark and Fritz, 1997; Dong, 2005; He, 2013). We used 85.00 pmC in the radiocarbon correction of Vogel Model.

Different ^{14}C -correction models consider different conditions and reactions in a groundwater system. The results of Vogel Model, Tamers Model, CMB Model and improved Pearson Model are similar, while the finding from F-G Model is slightly younger (Table 1). Overall, all models appear to be applicable to groundwater dating for the Longdong Loess Basin. Groundwater age of the Dongzhi Tableland ranges approximately from 3000 to 25,000a (Table S2), which is consistent with results from Huang et al. (2020).

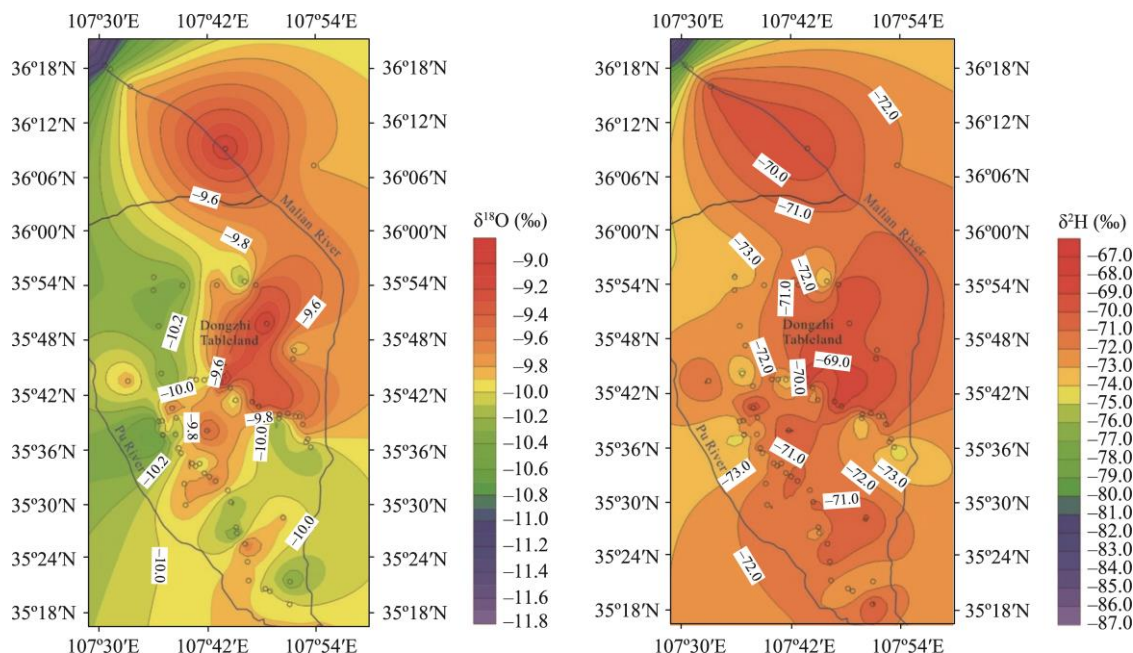


Fig. 6 Contour maps of the $\delta^{18}\text{O}$ (a) and $\delta^2\text{H}$ (b) of groundwater in the Longdong Loess Basin

A general trend is observed that groundwater becomes older as the water transports deeper from the land surface and farther from the center of the Dongzhi Tableland (Fig. 7) with a regression line:

$$z = 78.28x + 87.37y + 1700 \quad (R^2 = 0.57), \quad (1)$$

where x , y and z represent the distance from the center of the Dongzhi Tableland (km), depth from the land surface (m) and corrected ^{14}C age of groundwater (a), respectively. This is consistent with the hydrogeological background that the groundwater flows from the center to the margin of the Dongzhi Tableland (Pan et al., 2014). Using the relationship of groundwater age with depth and distance in Equation 1, a semi-quantitative estimation of groundwater age can be made for the Dongzhi Tableland, if depth and distance from the center are known. However, the groundwater system is more complicated than that described simply by the linear relationship. Hence, some groundwater samples do not follow the general trend, such as XF22, G30, G43 and G65 (younger than the predicted age by Eq. 1), and G22 (older than the predicted age by Eq. 1). Samples such as G30, G43 and G65 are close to the tributaries of the Malian River, which may recharge and interact with groundwater. XF22 is not far from the center and shallower than other groundwater samples, which may take the recharge from younger precipitation through preferential flow. G22 is quite far from the center and the river, resulting in a long flow path with an old age.

5 Discussion

5.1 Surface water system

The most conspicuous chemistry characteristics of surface water of the Malian River are its overall high salinity and the improving water quality along the flow path from northwest to southeast. There probably are two reasons for why the quality of surface water of the Malian

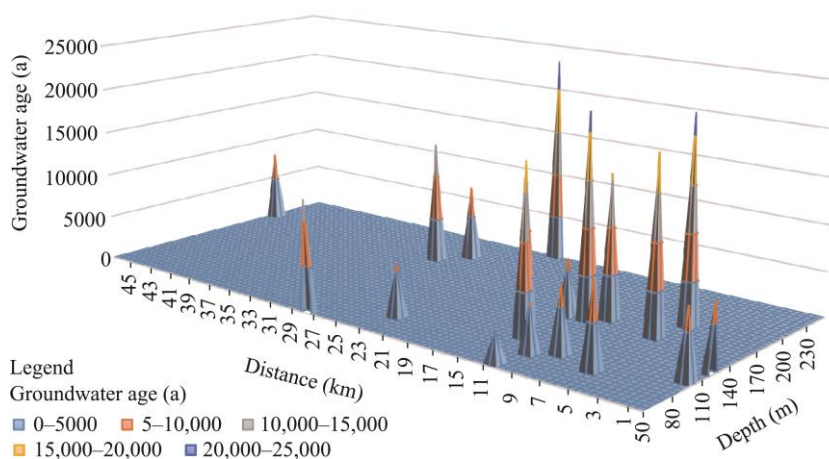


Fig. 7 Spatial distribution of groundwater ages in the Dongzhi Tableland

River becomes better from upstream, midstream to downstream. Firstly, the tributaries, which have better water quality and lower TDS (such as the Yuancheng River and Gucheng River), inflow into the main stream of the Malian River and the water yield becomes larger. Secondly, the leakage flow of groundwater in the Dongzhi Tableland with good quality discharges to the Malian River with flux of $1.65 \text{ m}^3/\text{s}$, accounting for 57.1% of the Malian River (Wang et al., 2018).

Figure 8 shows the trend of $\delta^{18}\text{O}$ of surface water and groundwater with the distance from the Malian River headwater, along with the stable isotope values of local precipitation at the river source ($\delta^{18}\text{O} = -7.90\text{‰}$ and $\delta^2\text{H} = -54.42\text{‰}$) (Su et al., 2009). The $\delta^{18}\text{O}$ values of surface water in the middle and lower reaches of the Malian River are between those of the local precipitation and groundwater along the river. Especially, in the river below the Maling Town, Qingcheng County, Gansu Province, the $\delta^{18}\text{O}$ values of surface water decrease and approach those of groundwater, indicating that the middle and lower reaches of the Malian River mainly receive the discharge from groundwater leakage, in addition to the tributaries, which is consistent with the results of Su et al. (2009). The chemical compositions also indicate the dilution effect of the Malian River water with groundwater (Fig. 4). However, the isotope compositions of the upstream of the Malian River are much closer to those of precipitation at the headwater ($\delta^{18}\text{O} = -7.90\text{‰}$ and $\delta^2\text{H} = -54.42\text{‰}$) than those of groundwater (Fig. 8), due to the limited hydraulic connection between the river and groundwater in the upstream (Su et al., 2009).

The upstream river water (SW6–SW8) has elevated isotopic compositions relative to the headwater (Fig. 8), which also deviates from the LMWL (Fig. 5). There are some reservoirs in the upstream of the Malian River, for example, Gaojiazhai Reservoir with the storage capacity of $4.40 \times 10^6 \text{ m}^3$ and Hujiagou Reservoir with the storage capacity of $5.25 \times 10^6 \text{ m}^3$. Considering an annual humidity of 53%, temperate continental monsoon climate and potential evaporation of 1380–1750 mm in Qingyang City, evaporation in these reservoirs is likely to cause the observed isotope enrichments. An isotopic composition of the initial surface water is assumed to be located at the intersection of an apparent evaporation line of surface water and the LMWL ($\delta^{18}\text{O} = -11.20\text{‰}$ and $\delta^2\text{H} = -78.00\text{‰}$), resulting in isotope enrichment of 4.40‰ and 19.00‰ for the $\delta^{18}\text{O}$ and $\delta^2\text{H}$, respectively. According to the slope (4.5) from surface water isotope value, which gives a humidity of 53.00%. The kinetic fractionation factor at the vapor-boundary layer (‰) is $\varepsilon^{18}\text{O}_{v-bl} = 14.2 \times (1-H)\text{‰} = 6.67\text{‰}$ (where v is the vapor; bl is the boundary layer; and H is the humidity (%)) (Gonfiantini, 1986). The equilibrium fractionation factor between water and vapor is $\varepsilon^{18}\text{O}_{w-v} = 10.60\text{‰}$ at temperature of 10.0°C (where w is the water) (Majoube, 1971). Therefore, the total fractionation factor of the ^{18}O ($\varepsilon^{18}\text{O}_{\text{total}}$) from liquid water to vapor is -17.27‰ . A fractional water loss by evaporation can be modeled by Rayleigh distillation, resulting in a 22.00% evaporation loss of surface water in the upstream of the Malian River. The intense evaporation-concentration process can explain the overall high salinity and poor quality of surface water in the Malian River

(SW1–SW8).

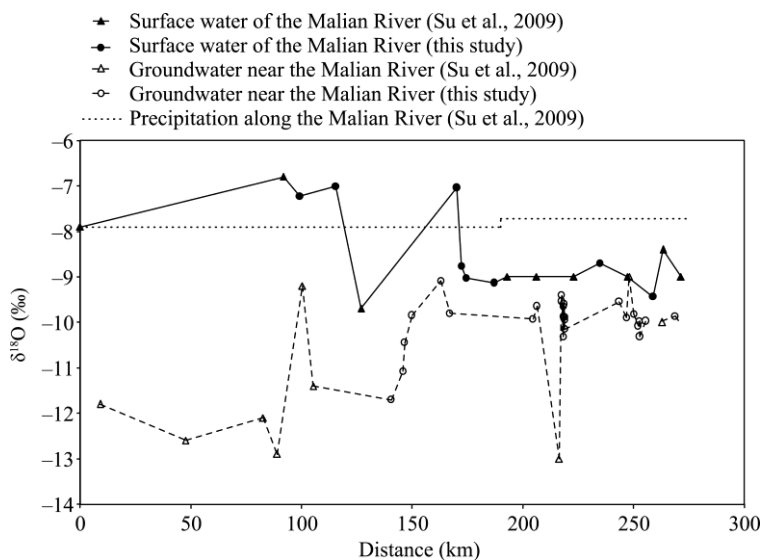


Fig. 8 Relationship between the $\delta^{18}\text{O}$ value of surface water, groundwater and precipitation and the distance from the headwater of the Malian River

5.2 Hydrogeochemical evolution of groundwater

In the Dongzhi Tableland, Ca^{2+} and Na^+ are the dominant cations of groundwater and HCO_3^- is the main anion, most likely due to the dissolution of carbonate minerals, as indicated by the saturation index of calcite. The concentration of Na^+ is between 0.38 and 35.26 mmol/L, while the total concentration of $\text{Ca}^{2+} + \text{Mg}^{2+}$ is between 0.30 and 12.99 mmol/L in groundwater of the Dongzhi Tableland. A general inverse relationship exists between the concentration of $\text{Ca}^{2+} + \text{Mg}^{2+}$ and the concentration of Na^+ , indicating cation exchange adsorption between Ca^{2+} and Mg^{2+} in groundwater and Na^+ on clay minerals (such as smectite) (Fig. S1). The two linear trends in the piper ion diagram also point to the cation exchange phenomenon (Fig. 3). It has also been shown that as the total concentration of $\text{Ca}^{2+} + \text{Mg}^{2+}$ decreases, the concentration of Na^+ in groundwater of the Quaternary Loess Aquifer increases (Ma et al., 2005a; Ding et al., 2009; He et al., 2011; Zhang et al., 2011; Ling, 2019; Ling et al., 2021). A good trend is observed that the ratio of $(\text{Ca}^{2+} + \text{Mg}^{2+})/\text{Na}^+$ decreases with the growth of corrected ^{14}C age of groundwater (Fig. 9), and an average cation exchange rate in groundwater of the Quaternary Loess Strata in the Dongzhi Tableland is $3.49 \times 10^{-5} \text{ mol}/(\text{L} \cdot \text{a})$, which means it will take 28,653 a for 1.00 mol $(\text{Ca}^{2+} + \text{Mg}^{2+})$ in per liter of groundwater exchanging with 2.00 mol Na^+ on clay minerals.

To better understand hydrogeochemical reactions occurring in groundwater of the Dongzhi Tableland, we conducted a reverse hydrogeochemical simulation, using Netpath XL1.4 (Plummer et al., 1991). Based on the groundwater level of the Longdong Loess Basin (Wang et al., 2018), we chose two groundwater flow paths: G35 to G47 in the east line and G2 to G22 in the south line of the Dongzhi Tableland.

From G35 to G47 in the east line, the concentrations of Na^+ and Ca^{2+} increase from 0.74 to 3.13 mmol/L and decrease from 1.35 to 0.59 mmol/L, respectively. The concentration of HCO_3^- increases from 3.44 to 3.79 mmol/L. There are little changes of other chemical compositions. Several possible models were tested by Netpath XL 1.4 (USGS, USA) with different combinations of mineral dissolution (calcite, albite, Na-montmorillonite and dolomite) and cation exchange with clays. The simulated ^{14}C concentrations at the starting point (sample G35) and estimated travel time are all similar to each other for the tested models. Based on the mineralogy of the Longdong Loess Basin (abundant albite relative to Na-montmorillonite and dolomite) and agreement of computed endpoint $\delta^{13}\text{C}$ values of DIC with the measured values (-7.91% vs. -7.12%), the model with the dissolution of calcite and albite and cation exchange is the most

likely simulation for the flow path from G35 to G47. According to this model, albite and calcite are dissolved (0.25 and 0.32 mmol/L, respectively), resulting in the increase of the concentrations of HCO_3^- , Ca^{2+} and Na^+ . Then, the dissolved Ca^{2+} in groundwater exchanges Na^+ on minerals (1.07 mmol/L), suggesting that cation exchange is the main reaction in the groundwater flow path. The simulated value of ^{14}C at G35 (27.43 pmC) and the measured ^{14}C value at G47 (3.94 pmC) give a travel time (16,041 a) between the two samples, which agrees well with the age difference between G35 and G47 (16,025 a), based on the corrected ^{14}C age of groundwater (Table 1).

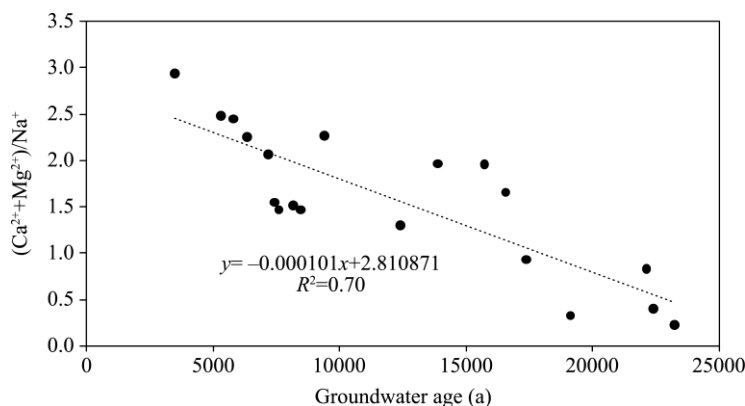


Fig. 9 Relationship between the ratio of $(\text{Ca}^{2+}+\text{Mg}^{2+})/\text{Na}^+$ and the ^{14}C age of groundwater

The simulation results for the flow path from G2 to G22 in the south line also show that the deposition of albite and calcite and cation exchange between $\text{Ca}^{2+}+\text{Mg}^{2+}$ and Na^+ takes place along the flow path. The simulated value of $\delta^{13}\text{C}_{\text{DIC}}$ at G22 is -9.08‰ , which is close to the measured value of -9.43‰ . Results show that it takes 4849 a for groundwater to flow from G2 to G22, which matches well with the age difference (4952 a) between G2 and G22. The reverse hydrogeochemical simulations for both the east and south line flow paths agree well with the ^{14}C age of groundwater and are consistent with the hydrogeological background that groundwater generally flows from the center towards the margin of the Dongzhi Tableland.

5.3 Groundwater hydrologic regime

Huang et al. (2020) estimated that a recharge time of precipitation to the groundwater table in the unconfined aquifer of the Dongzhi Tableland is approximately 220 a. Then, groundwater flows deeper and from the center to the margin of the Dongzhi Tableland, mainly to the east, south and west. Groundwater discharges as springs along many heavily incised galleys into rivers (the Malian River, the Puhe River and other rivers) at the flanks of the Dongzhi Tableland. A discharge flow from the Dongzhi Tableland groundwater to the Malian River was estimated $1.65 \text{ m}^3/\text{s}$, accounting for 57.1% of the Malian River (Wang et al., 2018).

The reverse hydrogeochemical simulation discussed above provides a migration time of 16,041 a from G35 to G47 with approximately 23 km in the east line, yielding an estimated flow velocity of 1.43 m/a . Based on this flow rate, the oldest groundwater in this Quaternary Loess Aquifer of the Dongzhi Tableland at the eastern margin is around 32,000 a. The oldest groundwater age and migration time from the center to the margin of the Dongzhi Tableland can also be estimated based on the age-depth-distance relationship (Eq. 1). As groundwater depth at the margin is approximately 300 m deep and the distance from the margin to the center is 40 km, the oldest groundwater age is nearly 31,050 (± 1000) a with an estimated average migration rate of 1.29 m/a . These estimated data agree well with those by the reversed hydrogeochemical simulation.

Migration time of groundwater can also be calculated by the hydraulic conductivity ($0.14\text{--}0.46 \text{ m/d}$) (Jia, 2010). According to the Darcy's Law, the flow velocity is $3.55 \times 10^{-4}\text{--}11.66 \times 10^{-4} \text{ m/d}$ with an average groundwater gradient of 2.50×10^{-3} . Then, it takes 65,000 to 213,000 a for groundwater to flow from the center to the margin of the Dongzhi Tableland. This migration time

is much longer than the estimates by the reverse hydrogeochemical simulation and the ^{14}C -based age-depth-distance relationship. The Darcy's Law assumes a laminar and piston-like water flow with the same hydraulic conductivity in the entire groundwater system, which suits well with homogeneous and isotropic geologic media. In reality, preferential flows with macropores and vertical fissures exist in loess aquifers, which may result in faster migration time and more complicated groundwater flow mechanism. In fact, some groundwater samples do not follow the general age trend. For example, XF22 is not far from the center and shallower than other groundwater samples, which may get the recharge from younger precipitation through preferential flow. Samples such as G30, G43 and G65 are close to the tributaries of the Malian River, and interactions with the river may result in younger ages.

5.4 Paleoclimate implications of groundwater

The isotopic compositions of modern precipitations in the Longdong Loess Basin have been well characterized: 2018–2019 in the Dongzhi Tableland (Huang et al., 2020), 1985–1993 in Xi'an and 2000–2001 at the Malian River headwater (Su et al., 2009) (Fig. 11). The annual weighted average isotopic compositions range from $\delta^{18}\text{O} = -8.50\text{‰}$ and $\delta^2\text{H} = -58.00\text{‰}$ (the Dongzhi Tableland) to $\delta^{18}\text{O} = -7.90\text{‰}$ and $\delta^2\text{H} = -54.42\text{‰}$ (the Malian River headwater) to $\delta^{18}\text{O} = -7.49\text{‰}$ and $\delta^2\text{H} = -49.13\text{‰}$ (Xi'an). However, it has been well recognized that the annual weighted average isotopic values of precipitation may not represent the water that infiltrates into the subsurface and eventually recharges groundwater in arid and semi-arid regions. Light precipitation may evaporate quickly from the surface before infiltration and heavy precipitation with distinct isotopic compositions is most likely to infiltrate deep into vadose zone. Precipitation data in 2018–2019 in the Dongzhi Tableland show that heavy summer precipitation from a summer monsoon season is approximately 1.00‰ depleted in the $\delta^{18}\text{O}$ relative to the annual weighted average value of the $\delta^{18}\text{O}$ (Huang et al., 2020). Isotope-enabled Global Circulation Model (GCM) also predicts that late monsoon (from July to October) precipitation in this region has lower $\delta^{18}\text{O}$ value ($< -8.00\text{‰}$) than the average (Hu et al., 2019). However, a much longer record from Xi'an station (1985–1993) shows the opposite, a heavier $\delta^{18}\text{O}$ value (-4.54‰) with heavy precipitation ($>50\text{ mm}$). Huang et al. (2020) reported isotopic compositions of soil water in the thick vadose zone in the Dongzhi Tableland. The $\delta^{18}\text{O}$ values are rather constant with the depth (0–55 m), ranging from -8.70‰ to -13.50‰ , with an average value of -10.54‰ . The $\delta^{18}\text{O}$ value at the groundwater table (45–55 m) is -10.00‰ , which may represent that of infiltrating water to groundwater in the recent past ($\leq 220\text{ a}$). This value of young groundwater is also consistent with the observed relationship between age and the $\delta^{18}\text{O}$ (Fig. 10). It appears that in the Longdong Loess Basin, late-monsoon heavy precipitation with depleted isotopic compositions penetrating the vadose zone could possibly contribute to groundwater recharge.

A negative relationship can be found between the $\delta^{18}\text{O}$ value and the corrected ^{14}C age of groundwater in the Dongzhi Tableland in this study:

$$y = -2.1 \times 10^5 x - 9.93 \quad (R^2 = 0.37), \quad (2)$$

where y is the $\delta^{18}\text{O}$ value (‰) and x is the groundwater age (a). The $\delta^{18}\text{O}$ value of groundwater becomes progressively lighter (around 0.48‰) with age between 3,000 and 23,000 a ago. Since during the Last Glacial Maximum (19,000–26,000 a ago), the ocean was enriched with the $\delta^{18}\text{O}$ (1.20‰) (Eagle et al., 2013), and the $\delta^{18}\text{O}$ of groundwater is about 1.68‰, lower than that of 2.3×10^4 a ago. The $\delta^{18}\text{O}$ value of modern precipitation is further greater (3.78‰–4.19‰) than groundwater after the correction of the Last Glacial Maximum ocean.

There are several possible processes that can cause the observed isotope depletion in groundwater. Hu et al. (2019) found that the changes in monsoon intensity in Southeast Asia influence the contributions and trajectories of moisture from different locations, affecting the $\delta^{18}\text{O}$ of precipitations. As nearly 60.00% of the annual precipitation occurs as rainstorms in July, August and September in the study area, heavy rains in summer and autumn contribute most to groundwater recharge as discussed above. In summer months, the main source of precipitation is from the Bay of Bengal (the Indian Ocean), southeast monsoon, westerly zone vapor and local re-evaporated water vapor (Liu et al., 2008, 2019). Air masses lose heavier isotopes during

travelling a long trajectory from the Indian Ocean to the inland in China. In addition, local re-evaporated water vapor may have contributed to the low isotopic compositions of groundwater. Apart from the changes of moisture sources, isotope composition is also an indicator of temperature. Depleted isotope values may indicate the colder temperature in rainout process in the Longdong Loess Basin.

According to the relationship between temperature and the $\delta^{18}\text{O}$ ($\delta^{18}\text{O}=0.695\times T_{\text{annual}}-13.6\text{‰}$, where T_{annual} is the annual average temperature ($^{\circ}\text{C}$)) (Dansgaard, 1964), the temperature in the Dongzhi Tableland during the Last Glacial Maximum is approximately 2.4°C – 6.0°C colder than the present. Our results are generally consistent with those derived from sub-fossil assemblages of chironomid head capsules (5.0°C colder in the Last Glacial Maximum) in Southeast China (Zhang et al., 2019), pollens (6.0°C – 10.0°C colder in the Last Glacial Maximum) in eastern China (Deng et al., 2002), lake records (-2.5°C to -17.5°C colder in the Last Glacial Maximum) in western China (Yu et al., 2003), clumped isotope thermometry of carbonates (6.0°C – 7.0°C colder in the Last Glacial Maximum) (Eagle et al., 2013) and snail shells (10.0°C colder in glacial time) on the Chinese Loess Plateau (Dong et al., 2020). The carbonate/shell-derived temperature records the temperature near the surface, while the groundwater-derived temperature may reflect overall condensation temperature in air masses. In addition, the $\delta^2\text{H}$ – $\delta^{18}\text{O}$ values of groundwater fall along a linear trend, which is slightly displaced compared to the modern LMWL (Fig. 5) with a lower deuterium excess value. Such a displacement in the $\delta^2\text{H}$ – $\delta^{18}\text{O}$ diagram may indicate a more humid climate in the source regions (the Bay of Bengal and South China Sea) during the last glacial time.

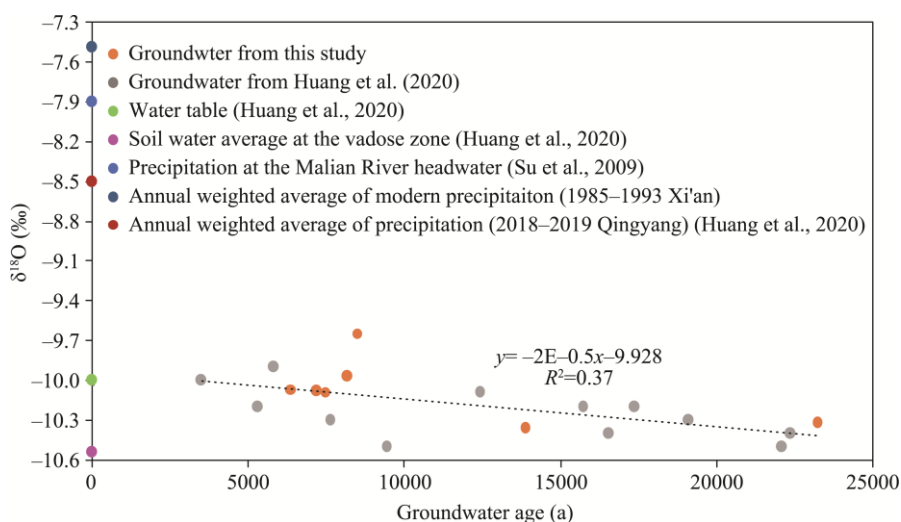


Fig. 10 Relationship between the $\delta^{18}\text{O}$ value and groundwater age along with modern precipitation

6 Conclusions

In the Longdong Loess Basin, groundwater in the Dongzhi Tableland and surface water along the Malian River show different hydrochemical characteristics. Groundwater of the Dongzhi Tableland is of a $\text{HCO}_3\text{--Ca--Na}$ type with low TDS ($<270\text{ mg/L}$). Dissolution of carbonate mineral and cation exchange among Ca^{2+} , Mg^{2+} and Na^+ are the main water-rock interaction in the groundwater system of the Dongzhi Tableland. Groundwater and surface water along the Malian River have high TDS, decreasing from northwest to southeast: cations are mainly Na^+ and K^+ , and anions are mainly Cl^- and SO_4^{2-} . Surface water in the middle and lower reaches of the Malian River receives the recharge mainly from groundwater on both sides of the valley, while the source of the Malian River mainly receives the recharge from local precipitation.

The main recharge of groundwater in the Longdong Loess Basin occurred in the Late Pleistocene and Holocene (3000 to 25,000 a ago), according to the corrected ^{14}C age of

groundwater, and there are some possibilities that late-monsoon heavy precipitation in the recent past (≤ 220 a) penetrating the unsaturated zone can contribute to groundwater recharge based on seasonal stable isotope signatures. Spatially, groundwater in the Dongzhi Tableland becomes older with increasing depth and distance from the center, while there is some mixing and interaction of old groundwater with younger water near the river tributaries. Groundwater migration rate is slow, about 1.29–1.43 m/a, and the oldest groundwater age is 32,000 a. Because of the ancient source and low renewability of groundwater in the Longdong Loess Basin, the issues of exploitation and management of groundwater resources should be paid more attention. The progressively decreasing $\delta^{18}\text{O}$ values of groundwater with the ages reflect that temperature is approximately 2.4 °C–6.0 °C colder in the Last Glacial Maximum than in the present, providing another evidence of climate change.

Acknowledgements

This research was supported by the National Natural Science Foundation of China (41271039), the Central University Basic Scientific Research Foundation of Innovation Personnel Training Project at Lanzhou University (lzujbky-2021-sp20, lzujbky-2017-it101) and the National Science Foundation of US to Dr. Juske HORITA (EAR 1804838, EAR 1836868). We acknowledge the valuable comments from two anonymous reviewers and the editors. We thank Dr. Reika YOKOCHI and Dr. Yesim DOLLAR for their helpful suggestions. We thank the researchers at Key Laboratory of Western China's Environmental System for their assistance. We also thank the researchers at Australian National University for their help in the ^{14}C measurements.

References

- Amanambu A C, Obarein O A, Mossa J, et al. 2020. Groundwater system and climate change: Present status and future considerations. *Journal of Hydrology*, 589: 125–163.
- Choi S U, Yoon B, Woo H. 2005. Effects of dam-induced flow regime change on downstream river morphology and vegetation cover in the Hwang River, Korea. *River Research and Applications*, 21(2–3): 315–325.
- Christensen N S, Wood A W, Voisin N, et al. 2004. Effects of climate change on the hydrology and water resources of the Colorado River basin. *Climatic Change*, 62(1): 337–363.
- Cigna F, Tapete D. 2021. Satellite InSAR survey of structurally-controlled land subsidence due to groundwater exploitation in the Aguascalientes Valley, Mexico. *Remote Sensing of Environment*, 254: 112254, doi: 10.1016/j.rse.2020.112254.
- Clark I D, Fritz P. 1997. *Environmental Isotopes in Hydrogeology*. Boca Raton: CRC Press, 153–154.
- Cochand M, Molson J, Barth J A C, et al. 2020. Rapid groundwater recharge dynamics determined from hydrogeochemical and isotope data in a small permafrost watershed near Umiujaq (Nunavik, Canada). *Hydrogeology Journal*, 28: 853–868.
- Conway D. 2005. From headwater tributaries to international river: Observing and adapting to climate variability and change in the Nile basin. *Global Environmental Change*, 15(2): 99–114.
- Cook P G, Herczeg A L. 2000. *Environmental Tracers in Subsurface Hydrology*. Boston: Springer, 72–73.
- Dansgaard W. 1964. Stable isotopes in precipitation. *Tellus*, 16(4): 436–468.
- Deng Y, Zheng Z, Cour P, et al. 2002. Relation between pollen ratios and climate in east China and an attempt of paleoclimate reconstruction. *Acta Palaeontologica Sinica*, 41(4): 508–516.
- Ding Z Y, Ma J Z, He J H. 2009. Geochemical evolution of groundwater in the southwest of Tengger desert, NW of China. *Arid Land Geography*, 32(6): 948–957. (in Chinese)
- Dong J B, Eiler J, An Z S, et al. 2020. Clumped and stable isotopes of land snail shells on the Chinese Loess Plateau and their climatic implications. *Chemical Geology*, 533: 119414, doi: 10.1016/j.chemgeo.2019.119414.
- Dong W H. 2005. Application of inverse hydrogeochemical modeling in ^{14}C age correction of deep groundwater in the Ordos Cretaceous Artesian Basin. PhD Dissertation. Changchun: Jilin University. (in Chinese)
- Eagle R A, Risi C, Mitchell J L, et al. 2013. High regional climate sensitivity over continental China constrained by glacial-recent changes in temperature and the hydrological cycle. *Proceedings of the National Academy of Sciences of the United States of America*, 110(22): 8813–8818.
- Edmunds W M, Guendouz A H, Mamou A. 2003. Groundwater evolution in the Continental Intercalaire aquifer of southern Algeria and Tunisia: trace element and isotopic indicators. *Applied Geochemistry*, 18(6): 805–822.
- Edmunds W M, Ma J Z, Aeschbach-Hertig W, et al. 2006. Groundwater recharge history and hydrogeochemical evolution in the Minqin Basin, North West China. *Applied Geochemistry*, 21(12): 2148–2170.

- Fontes J C, Garnier J M. 1979. Determination of the initial ^{14}C activity of the total dissolved carbon: A review of the existing models and a new approach. *Water Resources Research*, 15(2): 399–413.
- Gerber C, Vaikm   R, Aeschbach W, et al. 2017. Using ^{81}Kr and noble gases to characterize and date groundwater and brines in the Baltic Artesian Basin on the one-million-year timescale. *Geochimica et Cosmochimica Acta*, 205: 187–210.
- Godwin H. 1962. Half-life of radiocarbon. *Nature*, 195(4845): 984, doi: 10.1038/195984a0.
- Gonfiantini R. 1986. Environmental isotopes in lake studies. In: Fritz P, Fontes J C. *Handbook of Environmental Isotope Geochemistry*. Amsterdam: Elsevier, 113–168.
- He J H, Zhang J, Ding Z Y, et al. 2011. Evolution of groundwater geochemistry in the Minqin Basin: Taking chloride as an indicator of groundwater recharge. *Resources Science*, 33(3): 416–421. (in Chinese)
- He J H. 2013. The ^{14}C age correction of the groundwater in the Shule River Basin. PhD Dissertation. Lanzhou: Lanzhou University. (in Chinese)
- Hu J, Emile-Geay J, Tabor C, et al. 2019. Deciphering oxygen isotope records from Chinese speleothems with an isotope-enabled climate model. *Paleoceanography and Paleoclimatology*, 34(12): 2098–2112.
- Huang T M, Ma B Q, Pang Z H, et al. 2020. How does precipitation recharge groundwater in loess aquifers? Evidence from multiple environmental tracers. *Journal of Hydrology*, 583: 124532, doi: 10.1016/j.jhydrol.2019.124532.
- Jesija N P, Gopinath G, Resmi T R. 2021. Comprehending the groundwater recharge of a coastal city in humid tropical setting using stable isotopes. *Journal of Environmental Management*, 287: 112260, doi: 10.1016/j.jenvman.2021.112260.
- Jia B. 2010. Study on evolution of water quality and impact of oil development in the Malian River Basin of Longdong Loess Plateau. MSc Thesis. Lanzhou: Lanzhou University. (in Chinese)
- Jia W H, Yin L H, Zhang M S, et al. 2021. Quantification of groundwater recharge and evapotranspiration along a semi-arid wetland transect using diurnal water table fluctuations. *Journal of Arid Land*, 13(5): 455–469.
- Kinzelbach W, Bauer P, Siegfried T, et al. 2003. Sustainable groundwater management—problems and scientific tools. *Episodes*, 26(4): 279–284.
- Li C B, Qi J G, Wang S B, et al. 2014. A holistic system approach to understanding underground water dynamics in the Loess Tableland: A case study of the Dongzhi Loess Tableland in Northwest China. *Water Resources Management*, 28: 2937–2951.
- Li H X. 2015. Analysis of groundwater level change in recent 30 years in Dongzhi Tableland. *Ground Water*, 37(6): 63–64. (in Chinese)
- Li P C. 1999. Study on rational determination of specific yield in aquifer of loess area. *Journal of Hydraulic Engineering*, 11: 38–41. (in Chinese)
- Li W Y. 2013. Dynamics of underground water system and rational utilization of water resources in the Dongzhi Loess Tableland. MSc Thesis. Lanzhou: Lanzhou University. (in Chinese)
- Liang J N. 2011. Study on soil's heavy metal contents and soil quality evaluation of Longdong Tableland area. MSc Thesis. Lanzhou: Lanzhou University. (in Chinese)
- Ling X Y. 2019. Study on groundwater recharge and hydrogeochemical evolution of the loess plateau in East Gansu. MSc Thesis. Lanzhou: Lanzhou University. (in Chinese)
- Ling X Y, Ma J Z, Chen P Y, et al. 2021. Hydrogeochemical characteristics and radiocarbon dating of groundwater in the Dongzhi Tableland of Longdong Loess Plateau. *Journal of Lanzhou University (Natural Sciences)*, 57(1): 24–32. (in Chinese)
- Liu C M, Xia J. 2004. Water problems and hydrological research in the Yellow River and the Huai and Hai River basins of China. *Hydrological Processes*, 18: 2197–2210.
- Liu D S. 1985. *Loess and Environment*. Beijing: Science Press, 85–87. (in Chinese)
- Liu J R, Song X F, Yuan G F, et al. 2008. Characteristics of $\delta^{18}\text{O}$ in precipitation over Northwest China and its water vapor sources. *Acta Geographica Sinica*, 63(1): 12–22. (in Chinese)
- Liu J Y, Zhang F P, Feng Q, et al. 2019. Stable isotopes characteristics of precipitation over Shaanxi-Gansu-Ningxia and its water vapor sources. *Chinese Journal of Applied Ecology*, 30(7): 2191–2200. (in Chinese)
- Ma J Z, Chen F H, Zhao H. 2004. Groundwater recharge and climatic change during the last 1000 years from unsaturated zone of SE Badain Jaran Desert. *Chinese Science Bulletin*, 49(14): 22–26. (in Chinese)
- Ma J Z, Li X H, Huang T M, et al. 2005. Chemical evolution and recharge characteristics of water resources in the Shiyang River Basin. *Resources Science*, 27(3): 117–122. (in Chinese)
- Ma J Z, Edmunds W M. 2006. Groundwater and lake evolution in the Badain Jaran Desert ecosystem, Inner Mongolia. *Hydrogeology Journal*, 14: 1231–1243.
- Ma J Z, Pan F, Chen L H, et al. 2010. Isotopic and geochemical evidence of recharge sources and water quality in the Quaternary aquifer beneath Jinchang city, NW China. *Applied Geochemistry*, 25(7): 996–1007.
- Ma J Z, He J H, Qi S, et al. 2013. Groundwater recharge and evolution in the Dunhuang Basin, northwestern China. *Applied*

- Geochemistry, 28: 19–31.
- Magilligan F J, Nislow K H. 2005. Changes in hydrologic regime by dams. *Geomorphology*, 71(1–2): 61–78.
- Majoube M. 1971. Oxygen-18 and deuterium fractionation between water and steam. *Journal de Chimie Physique et de Physico-Chimie Biologique*, 68: 1423–1436. (in French)
- Murad A A, Garamoon H, Hussein S, et al. 2011. Hydrogeochemical characterization and isotope investigations of a carbonate aquifer of the northern part of the United Arab Emirates. *Journal of Asian Earth Sciences*, 40(1): 213–225.
- Obeidat M, Awawdeh M, Al-Kharabsheh N, et al. 2021. Source identification of nitrate in the upper aquifer system of the Wadi Shueib catchment area in Jordan based on stable isotope composition. *Journal of Arid Land*, 13(4): 350–374.
- Pan F, Chen L H, Fu S J, et al. 2012. A study on the transport performance of the petroleum contaminants in soil of the Longdong loess plateau. *Acta Scientiae Circumstantiae*, 32(2): 410–418. (in Chinese)
- Pan F, Zhang Q H, He J H. 2014. Groundwater recharge environment and geochemistry evolution of the Quaternary aquifer in the Dongzhiyuan region, Gansu Province. *Arid Land Geography*, 37(1): 9–18. (in Chinese)
- Pang Y J, Zhang H, Cheng H H, et al. 2020. The modulation of groundwater exploitation on crustal stress in the North China Plain, and its implications on seismicity. *Journal of Asian Earth Sciences*, 189: 104141, doi: 10.1016/j.jseas.2019.104141.
- Patil N S, Chetan N L, Nataraja M, et al. 2020. Climate change scenarios and its effect on groundwater level in the Hiranyakeshi watershed. *Groundwater for Sustainable Development*, 10: 100323, doi: 10.1016/j.gsd.2019.100323.
- Pearson F J, Hanshaw B B. 1970. Sources of dissolved carbonate species in groundwater and their effects on carbon-14 dating. In: I.A.E.A. Symposium on the Use of Isotopes in Hydrology. Vienna: International Atomic Energy Agency, 9–13.
- Plummer L N, Prestemon E C, Parkhurst D L. 1991. An interactive code (NETPATH) for modeling net geochemical reactions along a flow path. In: *Water-Resource Investigations Report 91–4078*. Department of the Interior, US Geological Survey. Reston, USA.
- Qu H L. 1991. *China Arid and Semi-arid Areas Groundwater Resources Assessment*. Beijing: Science Press. (in Chinese)
- Ragab R, Prudhomme C. 2002. SW—soil and water: climate change and water resources management in arid and semi-arid regions: Prospective and challenges for the 21st century. *Biosystems Engineering*, 81(1): 3–34.
- Shiklomanov I A, Rodda J C. 2003. *World Water Resources at the Beginning of the Twenty-First Century*. Cambridge: Cambridge University Press, 289–290.
- Sklash M G. 1990. Environmental isotope studies of storm and snow melt runoff generation. In: Anderson M G, Burt T P. *Process Studies in Hillslope Hydrology*. Hoboken: John Wiley & Sons Inc., 401–436.
- Su X S, Wan Y Y, Dong W H, et al. 2009. Hydraulic relationship between Malianhe River and groundwater: Hydrogeochemical and isotopic evidences. *Journal of Jilin University (Earth Science Edition)*, 39(6): 1087–1094. (in Chinese)
- Su Y H, Zhu G F, Feng Q, et al. 2009. Chemical evolution of shallow groundwater and the residence time in the Ejina Basin. *Arid Land Geography*, 32(4): 544–551. (in Chinese)
- Tamers M A. 1966. Instituto venezolano de investigaciones cientificas natural radiocarbon measurements II. *Radiocarbon*, 8: 204–212.
- Vogel J C. 1967. Investigation of groundwater flow with radiocarbon. In: *Symposium on Isotopes in Hydrology*. Vienna: International Atomic Energy Agency, 355–369.
- Walling D E, Fang D. 2003. Recent trends in the suspended sediment loads of the world's rivers. *Global and Planetary Change*, 39(1–2): 111–126.
- Wang P, Zhang F E, Chen Z Y. 2020. Characterization of recharge processes and groundwater flow paths using isotopes in the arid Santanghu basin, Northwest China. *Hydrogeology Journal*, 28: 1037–1051.
- Wang W H, Chen Y N, Wang W R. 2020. Groundwater recharge in the oasis-desert areas of northern Tarim Basin, Northwest China. *Hydrology Research*, 51(6): 1506–1520.
- Wang Y, Liu R Q. 2005. Groundwater resources in Dongzhiyuan and its sustainable utilization. *Water Resources Protection*, 21(1): 64–66. (in Chinese)
- Wang Y S, Cheng X X, Zhang M N, et al. 2018. Tracing the interactions between river water and groundwater in the lower reaches of Malian River. *Water Resources and Power*, 36(9): 48–51. (in Chinese)
- Wheater H S, Tompkins J A, van Leeuwen M, et al. 2010. Uncertainty in groundwater flow and transport modelling—a stochastic analysis of well-protection zones. *Hydrological Processes*, 14(11–12): 2019–2029.
- Xia J, Zhang Y Y. 2008. Water security in north China and countermeasure to climate change and human activity. *Physics and Chemistry of the Earth, Parts A/B/C*, 33(5): 359–363.
- Ye B S, Yang D Y, Kane D L. 2003. Changes in Lena River streamflow hydrology: Human impacts versus natural variations. *Water Resources Research*, 39(7): 1200–1214.
- Yu G, Xue B, Liu J, et al. 2003. LGM lake records from China and an analysis of climate dynamics using a modelling approach.

- Global and Planetary Change, 38(3–4): 223–256.
- Zhang E L, Chang J, Shulmeister J, et al. 2019. Summer temperature fluctuations in Southwestern China during the end of the LGM and the last deglaciation. *Earth and Planetary Science Letters*, 509: 78–87.
- Zhang Q H, Zhang Y R, Zhao Y P, et al. 2011. Geochemical evolution of groundwater and hydrogeochemical modeling in Jinta Basin. *Arid Land Geography*, 34(5): 772–778. (in Chinese)
- Zhang Q H, Luo Z X, Lu W, et al. 2020. Using water isotopes and hydrogeochemical evidences to characterize groundwater age and recharge rate in the Zhangjiakou area, North China. *Journal of Geographical Sciences*, 30: 935–948.
- Zheng H H, Theng B K G, Whitton J S. 1994. Mineral composition of Loess-Paleosol samples from the Loess Plateau of China and its environmental significance. *Chinese Journal of Geochimica*, 13: 61–72.
- Zhu G F, Su Y H, Feng Q. 2008. The hydrogeochemical characteristics and evolution of groundwater and surface water in the Heihe River Basin, northwest China. *Hydrogeology Journal*, 16: 167–182.

Appendix

Table S1 Concentrations of chemical ions and values of the $\delta^2\text{H}$ and $\delta^{18}\text{O}$ of groundwater (G) and surface water (SW) samples in the Longdong Loess Basin

Sample No.	Depth (m)	pH	TDS (mg/L)	Ca ²⁺ (mg/L)	Mg ²⁺ (mg/L)	Na ⁺ (mg/L)	K ⁺ (mg/L)	HCO ₃ ⁻ (mg/L)	Cl ⁻ (mg/L)	SO ₄ ²⁻ (mg/L)	NO ₃ ⁻ (mg/L)	F ⁻ (mg/L)	$\delta^2\text{H}$ (‰)	$\delta^{18}\text{O}$ (‰)
G1	120	8.47	246	37.43	12.91	17.24	1.38	275	7.65	2.50	4.23	0.07	-68.77	-9.54
G2	120	7.07	254	51.60	4.71	22.06	0.71	231	4.73	4.84	9.37	0.42	-72.03	-10.08
G3	130	7.84	261	41.85	14.46	9.37	1.29	270	3.89	2.47	3.12	0.06	-71.57	-9.85
G4	80	7.83	255	65.44	6.26	21.82	0.30	281	5.80	7.52	13.15	0.00	-73.65	-10.52
G5	150	8.30	230	55.96	5.06	23.73	0.45	265	4.31	6.15	7.63	0.28	-69.70	-9.41
G6	110	8.02	240	35.38	12.56	20.20	1.65	267	3.10	1.46	3.88	0.07	-71.72	-9.77
G7	160	7.80	252	62.64	5.56	29.15	0.53	274	4.92	7.01	13.64	0.00	-74.43	-10.61
G8	180	8.11	236	32.51	3.27	72.55	0.39	271	4.41	5.14	9.47	0.00	-73.33	-10.24
G9	130	8.15	221	18.20	7.57	37.10	0.93	263	2.38	0.98	3.52	0.11	-70.54	-9.81
G10	80	7.45	246	51.78	4.89	17.56	0.79	240	3.07	3.47	8.09	0.34	-73.17	-10.04
G11	350	8.50	240	40.47	14.76	12.26	1.57	259	4.62	3.08	4.70	0.06	-71.22	-9.71
G12	185	8.14	256	57.49	5.83	34.29	0.51	292	5.69	4.63	13.80	0.35	-72.05	-9.91
G13	114	7.97	230	32.70	2.97	44.65	0.92	238	3.43	2.57	9.14	0.41	-71.92	-10.11
G14	110	8.26	252	59.54	6.02	29.93	0.47	308	3.87	5.43	10.39	0.27	-71.66	-9.89
G15	130	8.19	224	39.08	13.52	10.39	1.50	287	3.34	1.66	3.01	0.07	-70.22	-9.64
G16	120	8.30	224	48.02	4.26	19.14	0.75	227	3.30	3.19	8.29	0.35	-70.50	-9.64
G17	120	8.15	238	58.45	5.08	24.78	0.73	271	4.47	6.36	10.80	0.31	-71.78	-9.80
G18	130	7.67	236	46.71	4.14	20.21	0.79	221	3.03	3.14	6.26	0.31	-70.94	-9.79
G19	160	7.98	229	29.59	9.74	26.16	1.83	257	5.24	1.53	8.75	0.09	-72.10	-9.92
G20	114	8.38	221	37.91	3.14	36.46	0.49	231	3.18	3.52	6.69	0.43	-70.83	-10.23
G21	190	8.11	232	45.99	4.11	19.70	0.60	223	2.78	2.81	6.05	0.35	-69.83	-9.88
G22	48	7.99	249	47.86	3.83	24.08	0.51	230	3.19	3.12	7.65	0.34	-71.57	-10.09
G23	100	8.55	249	40.49	3.13	36.77	0.76	230	3.86	2.58	8.18	0.44	-73.14	-10.50
G24	110	8.24	243	45.12	14.47	9.61	0.93	298	3.62	3.26	3.35	0.07	-69.87	-9.55
G25	100	8.32	244	47.20	4.32	23.66	0.60	240	5.66	4.02	3.19	0.38	-70.74	-9.90
G26	130	8.18	236	26.79	10.06	33.28	1.70	287	3.35	1.54	2.11	0.11	-71.88	-9.82
G27	150	8.32	244	22.49	2.55	60.12	0.86	256	2.66	2.25	0.24	2.25	-72.94	-10.08
G28	150	8.16	236	17.86	7.83	42.66	2.08	281	3.81	1.00	1.92	0.13	-72.94	-9.97
G29	100	8.63	227	41.75	3.96	28.27	0.50	223	3.60	3.88	5.67	1.71	-72.95	-10.31
G30	200	8.48	246	46.52	4.54	20.59	0.63	226	2.95	3.85	5.96	0.37	-69.76	-9.97
G31	100	7.53	340	14.59	7.20	45.70	1.72	249	6.20	6.60	2.19	0.15	-72.40	-9.87
G32	150	8.02	234	52.14	4.26	16.15	0.72	219	3.14	3.70	6.07	0.35	-70.76	-9.79
G33	135	8.21	248	31.24	2.78	47.23	0.49	235	4.26	2.64	14.28	0.55	-74.56	-10.27
G34	151	8.18	227	28.22	2.60	43.77	0.62	226	3.08	2.10	8.94	0.55	-72.92	-10.29
G35	92	8.30	240	53.98	4.18	16.95	0.46	210	5.76	4.55	13.12	0.39	-71.36	-10.08
G36	110	8.31	220	40.94	3.66	25.05	0.61	215	4.11	3.73	9.55	0.47	-70.66	-10.04
G37	300	7.81	246	31.24	10.98	18.88	1.14	248	5.24	1.75	6.47	0.06	-73.29	-9.94
G38	110	7.92	220	28.48	10.01	22.64	1.60	255	3.76	1.91	2.98	0.07	-73.49	-9.94
G39	150	7.96	241	28.97	12.49	43.82	1.60	236	7.71	1.90	14.29	0.10	-76.64	-10.39
G40	75	8.57	242	31.22	2.87	44.16	0.90	230	3.38	3.20	11.01	0.47	-72.17	-10.05
G41	150	8.49	150	10.91	4.32	28.50	1.25	187	3.12	2.02	4.17	0.11	-65.76	-8.53
G42	100	8.93	220	38.66	13.28	11.00	1.77	259	5.24	2.36	3.16	0.06	-72.26	-9.79
G43	150	8.04	266	54.40	4.84	15.96	0.32	223	3.22	15.99	9.32	0.39	-72.17	-10.06
G44	155	7.96	250	37.84	12.92	10.99	1.62	240	3.48	1.76	3.49	0.07	-68.48	-9.37

To be continued

JOURNAL OF ARID LAND

Continued

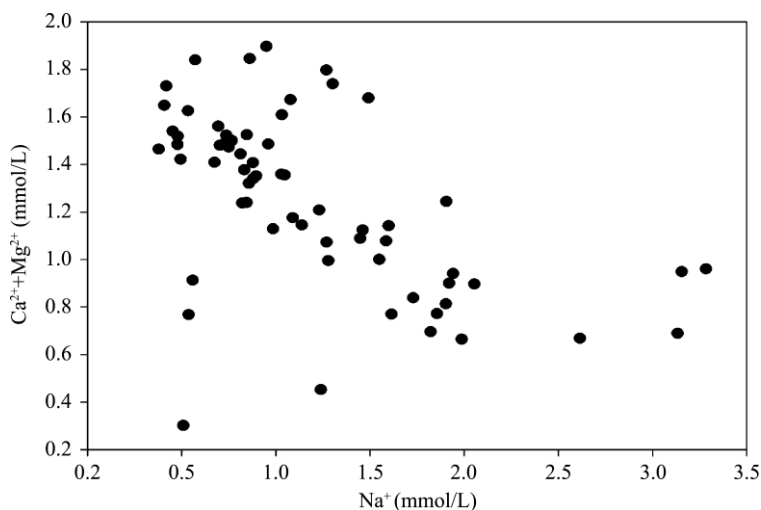
Sample No.	Depth (m)	pH	TDS (mg/L)	Ca ²⁺ (mg/L)	Mg ²⁺ (mg/L)	Na ⁺ (mg/L)	K ⁺ (mg/L)	HCO ₃ ⁻ (mg/L)	Cl ⁻ (mg/L)	SO ₄ ²⁻ (mg/L)	NO ₃ ⁻ (mg/L)	F ⁻ (mg/L)	δ ² H (‰)	δ ¹⁸ O (‰)
G45	180	8.73	224	35.52	12.82	11.35	1.04	243	3.44	1.71	3.59	0.06	-68.65	-9.35
G46	110	8.33	234	15.60	7.35	41.90	1.43	269	3.41	1.60	3.18	0.10	-71.69	-9.53
G47	250	8.39	266	23.66	2.35	72.05	1.82	231	2.41	2.41	4.39	0.57	-74.37	-10.32
G48	170	8.07	228	25.50	10.47	29.18	1.61	270	3.14	1.50	3.07	0.10	-69.45	-9.41
G49	100	8.34	211	34.38	3.25	29.39	0.77	210	1.90	3.85	7.57	0.64	-72.39	-9.88
G50	90	8.18	199	22.32	8.52	12.83	1.47	223	2.36	1.49	3.01	0.07	-71.21	-9.65
G51	120	8.13	210	36.96	12.98	8.69	0.97	249	2.85	2.30	3.28	0.06	-70.53	-9.59
G52	120	8.11	137	18.86	7.13	12.34	1.26	155	4.42	3.09	1.65	0.05	-72.65	-9.88
G53	200	8.26	226	28.06	3.30	39.75	0.56	206	2.54	2.68	6.42	0.55	-72.20	-9.94
G54	110	8.30	78	8.91	1.91	11.68	1.21	127	4.60	3.92	1.06	0.03	-74.72	-10.15
G55	145	7.86	251	49.70	4.85	18.67	0.45	219	2.93	4.30	6.69	0.31	-72.32	-10.22
G56	180	8.12	267	53.20	4.68	19.45	0.42	226	5.57	3.68	20.53	0.41	-72.68	-10.33
G57	150	8.68	241	39.43	3.34	33.59	0.65	224	3.66	2.71	10.35	0.47	-72.77	-10.31
G58	100	7.30	239	65.63	4.79	13.14	2.21	263	3.49	5.75	9.70	0.41	-74.10	-10.26
G59	190	7.86	251	52.79	4.38	17.59	0.63	230	2.58	3.33	7.00	0.28	-72.58	-10.36
G60	110	8.02	249	52.12	4.37	16.52	0.58	230	4.00	4.08	7.82	0.36	-70.13	-9.67
G61	263	8.14	249	32.24	3.71	75.53	0.74	288	3.43	4.19	5.63	0.35	-74.78	-10.26
G62	180	8.17	235	49.19	4.31	15.49	0.53	215	3.41	4.20	4.96	0.31	-69.26	-9.44
G63	75	7.81	246	64.51	5.59	19.80	0.32	261	5.22	12.16	10.73	0.30	-69.59	-9.05
G64	170	8.19	227	35.14	2.93	35.62	0.58	220	3.95	3.79	9.79	0.38	-70.75	-9.93
G65	210	8.13	226	43.03	3.94	19.43	0.66	212	2.35	3.14	5.89	0.31	-69.32	-9.64
G66	15	7.67	576	51.02	11.90	148.25	1.79	271	72.13	144.98	12.18	0.90	-72.01	-9.80
G67	26	7.71	457	47.73	12.06	103.38	1.57	324	41.56	45.62	37.00	0.58	-68.95	-9.09
G68	13	7.95	998	120.45	27.58	133.70	7.70	200	315.61	138.47	46.02	0.00	-69.84	-9.85
G69	7	7.90	970	75.80	20.68	234.80	1.69	346	234.31	215.99	13.27	0.00	-74.83	-10.45
G70	12	7.83	1189	97.80	26.24	274.78	1.61	287	295.11	306.65	34.27	0.00	-78.57	-11.08
G71	10	7.67	3410	335.66	110.41	810.95	9.16	283	818.72	1462.75	221.53	0.00	-86.15	-11.70
SW1	-	8.39	899	63.61	69.42	138.98	7.17	194	139.26	145.29	5.96	0.00	-72.03	-9.44
SW2	-	8.96	1236	70.76	77.97	166.52	9.43	229	175.00	170.69	7.20	0.00	-66.74	-8.70
SW3	-	8.42	2080	99.19	137.49	269.72	9.11	193	360.30	289.45	15.49	0.00	-70.68	-9.13
SW4	-	8.48	2380	157.79	56.77	629.95	4.50	232	759.60	769.55	60.16	0.00	-70.57	-9.03
SW5	-	8.70	816	57.65	16.63	217.33	1.88	261	157.55	203.30	7.79	0.94	-66.28	-8.76
SW6	-	8.64	2760	197.07	71.14	709.39	3.21	225	832.62	816.81	78.03	0.00	-59.13	-7.04
SW7	-	8.41	1533	127.55	34.52	410.63	3.84	260	397.98	472.77	27.54	0.00	-59.70	-7.01
SW8	-	8.36	7330	654.38	218.79	1843.86	12.95	162	2647.73	2214.16	292.63	0.00	-64.30	-7.23

Note: No., number; TDS, Total dissolved solids; -, no data.

Table S2 ^{14}C age of groundwater

Sample No.	Vogel Model	Tamers Model	CMB Model	Improved Pearson Model	F-G Model	Average age (a)	Uncorrected ^{14}C age	Huang et al. (2020)
G2	8870	7835	9622	6634	4656	7452±2796	9925±37	-
G22	13,717	12,682	14,149	11,794	9675	12,404±2728	14,635±60	-
G30	9641	8607	10,219	6673	5816	8191±2375	10,675±39	-
G35	8621	7586	9805	5974	4021	7201±3181	9680±36	-
G43	7803	6768	8491	4765	3992	6364±2372	8900±35	-
G47	25,392	24,357	25,788	21,146	19,447	23,226±3779	25,980±120	-
G59	15,272	14,238	15,705	12,927	11,179	13,864±2685	16,150±54	-
G65	9790	8755	10,896	6890	6027	8472±2444	10,815±45	-
XF3	19,333	18,298	16,607	17,557	15,104	17,380±2276	-	14,074
XF5	21,253	20,218	18,981	18,275	16,867	19,119±2252	-	15,995
XF6	7551	6516	4536	4371	3608	5316±1709	-	2293
XF9	18,563	17,528	16,240	16,345	14,083	16,552±2469	-	13,305
XF11	17,692	16,657	15,065	15,565	13,607	15,717±2110	-	12,434
XF14	24,479	23,444	22,207	21,794	20,037	22,392±2355	-	19,220
XF16	9793	8758	7392	6913	5182	7608±2425	-	4535
XF20	24,111	23,077	22,184	21,710	19,502	22,117±2615	-	18,853
XF22	7923	6888	5995	4844	3469	5824±2354	-	2665
XF24	11,558	10,524	8857	8969	7165	9415±2249	-	6300
XF25	5481	4446	3717	2892	947	3497±2550	-	220

Note: The typical uncertainty of the ^{14}C age is 500 a for Vogel Model, 200 a for Tamers Model, 70 a for CMB Model, 500–600 a for Improved Pearson Model and 50 a for F-G Model. CMB, chemical mass balance; F-G, Fontes-Garnier; XF, Xifeng District; -, no data. Mean±SD.

**Fig. S1** Relationship between the concentration of $\text{Ca}^{2+}+\text{Mg}^{2+}$ and Na^{+} in groundwater of the Dongzhi Tableland